AIAA JOURNAL
Vol. 45, No. 5, May 2007

Novel Signal Wave Pattern for Efficient Synthetic Jet Generation

P. F. Zhang* and J. J. Wang†
Beijing University of Aeronautics and Astronautics, 100083 Beijing, People's Republic of China

DOI: 10.2514/1.25445

A novel signal wave pattern is proposed to generate a more efficient synthetic jet, and the unsteady and mean flow characteristics of the synthetic jet generated by different suction duty cycle factors k are examined by numerical simulation. The mean flowfields of the synthetic jet with different k have similar features to that exhibited in previous experiments, but they would have a stronger and larger scale vortex pair with a larger suction duty cycle factor k, when the two key parameters, the stroke length ratio L_0/D and the Reynolds number Re_{U_0} (based on the characteristic blowing velocity U_0 and the orifice scale D), are set to be constant. The suction duty cycle factor k affects the vortex strength formed during the blowing cycle only, and nearly does not influence the convection velocity and trajectory of the vortex. During the suction cycle, the entrainment effect of the actuator decreases with the increase of suction duty cycle factor k, so that the vortex pair can propagate farther and coalesce to synthesize a larger scale jet.

I. Introduction

THE synthetic jet was found by Ingard and Labate [1] in 1950. They used standing waves in an acoustically driven circular tube to induce an oscillating velocity field in the vicinity of an orifice endplate and observed the formation of zero net mass flux jets from opposing trains of vortex rings on both sides of the orifice. It has been a popular laboratory flow control method since it was first used by Glezer and Amitay [2] in 1994. The synthetic jet is a zero-net-mass-flux jet which transfers linear momentum to the flow system without net mass injection across the flow boundary. The synthetic jets are usually produced by a sinusoidal oscillating membrane or piston to alternatively force fluid through an orifice into the external flowfield and entrain fluid back. During the blowing cycle, the ejected fluid separates at the sharp edges of the orifice and rolls up to form a vortex ring or vortex pair. When the membrane begins its suction cycle, the vortex pair is quite far from the orifice and keeps on propagating away due to its self-induced velocity. Hence, the vortex pair would not be entrained to the cavity, but it will coalesce to synthesize a jet with momentum transfer to the embedding flow. The synthetic jet has a unique feature compared with the traditional blowing or suction flow control methods, which is that the synthetic jet requires neither the external air supply nor the complex piping. The synthetic jet actuator has some advantages such as reduced size and weight, improved manufacturability, low cost, and increased reliability, so it has attracted more and more attention in the last two decades. With the development of microelectromechanical systems [3], the synthetic jet will be more attractive in flow control of both external and internal flows (see [4–9]).

Plenty of experiments have been carried out to study the vortex formation and evolution of the synthetic jet with circular or two-dimensional orifices (see [10–14]). Two parameters have been found to be the keys to determine the synthetic jet formation. One is the stroke length ratio L_0/D:

$$L_0 = \int_0^{\tau} u(t)\,\mathrm{d}t$$

where $u(t)$ is the streamwise velocity averaged along the cross-stream direction of the orifice, τ is the time length of blowing cycle, and D is the characteristic length scale of the orifice. The other parameter is the Reynolds number based on the blowing cycle (i.e., the characteristic velocity associated with the blowing cycle) and is given by $Re_{U_0} = U_0 D/\nu$, where $U_0 = L_0 f$ (f is the oscillation frequency of the actuator). In the formation of the synthetic jet, the stroke length ratio L_0/D influences the convection velocity and trajectory of the vortex, and the Reynolds number Re_{U_0} determines the vortex strength. In the far field, the synthetic jet bears much resemblance to the continuous jet. However, in the near field, thesynthetic jet entrains more fluid and thus grows faster than the continuous jet. Shuster and Smith [14], and Holman et al. [15] discussed the criterion condition to form a synthetic jet based on a simple "slug" model [15], and they argued that the synthetic jet formation is governed by the self-induced velocity of the vortex formed during blowing cycle V_I and the averaged velocity during the suction cycle V_s. When V_1/V_s is set larger than K, here K is a constant, the synthetic jet will be formed. By order analysis of the magnitude, it follows that

$$\frac{V_I}{V_s} \sim \frac{Re}{S} > K, \qquad Re = \bar{U}D/\nu, \qquad S = \sqrt{\frac{2\pi f D^2}{\nu}}$$

where Re is the Reynolds number based on the spatial and temporal averaged velocity during blowing cycle $\bar{U}$ and the length scale of the orifice D, and S is the Stokes number of the actuator frequency. The data support that the constant K is approximately 2.0 and 0.16 for two-dimensional and axisymmetrical synthetic jets, respectively.

In the applications of the synthetic jet actuation, it is required to increase the efficiency of the synthetic jet control. Smith et al. [16] used adjacent synthetic jet actuators driven by signals with different phase angles to generate jet vector, which improved the effect of the synthetic jet on separation control. Guy et al. [17] carried out experimental study on the effects of the geometry parameters to the velocity field of the synthetic jet. The cavity depth, orifice width, lip thickness, and orifice vertex angle were examined. Milanovic and Zaman [18], and Zhong et al. [19] investigated the influence of the orifice pitching and skew angles on the synthetic jet formation. They found that the increase in orifice pitching angle leads to a higher jet exit velocity and more asymmetrical rolling up of vortex rings, then they suggested that a pitching angle of 45 deg could be a more desirable choice for the actuator configuration design.

In previous studies, a lot of actuator signals were used to produce the synthetic jet, such as the sinusoidal wave [4–8], the square wave [20], and the sawtooth wave [21]. To improve the flow control effect, they even used the amplitude modulation on the sinusoidal wave [22]. We have understood that the condition for the synthetic jet formation is that the self-induced velocity of the vortex formed during blowing cycle V_I is larger than the averaged velocity during the suction cycle V_s from the preceding discussion. Hence, the vortex formed during the blowing cycle would not be entrained back to the

Received 25 May 2006; revision received 29 November 2006; accepted for publication 12 February 2007. Copyright © 2007 by the American Institute of Aeronautics and Astronautics, Inc. All rights reserved. Copies of this paper may be made for personal or internal use, on condition that the copier pay the $10.00 per-copy fee to the Copyright Clearance Center, Inc., 222 Rosewood Drive, Danvers, MA 01923; include the code 0001-1452/07 $10.00 in correspondence with the CCC.

*Postdoctor, Institute of Fluid Mechanics, Beijing; pfzhang@buaa.edu.cn.
†Professor, Institute of Fluid Mechanics, Beijing; jjwang@buaa.edu.cn.

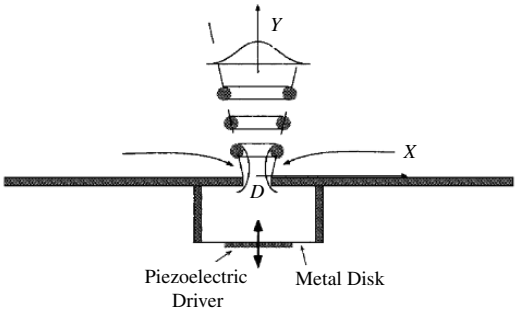

a) Vortex formation and evolution

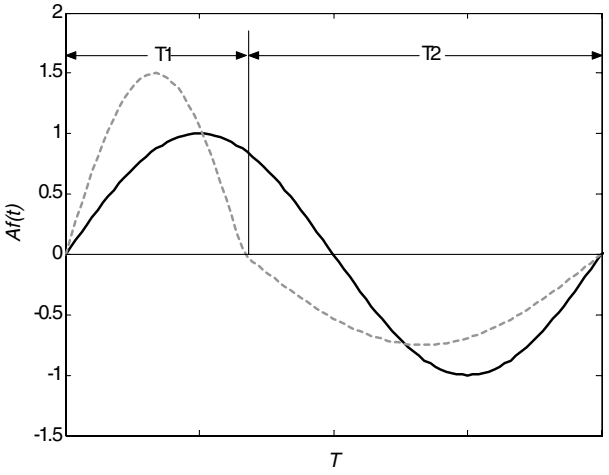

b) Signal wave pattern

Fig. 1 Diagram sketch of the formation of the synthetic jet and the signal wave pattern with some parameter definitions.

cavity during suction cycle, if the time scale of the suction cycle is increased, and the mass flux stays the same as that during the blowing cycle (as shown in Fig. 1b, the dashed line). In this case, it is expected that if the vortex formed during the blowing cycle has equal strength as that generated by the standard sinusoidal function, the entrainment of the orifice during the suction cycle on the vortex would be decreased, thus the vortex may propagate farther and form a more efficient synthetic jet. In this paper, we propose a novel signal wave pattern to generate a more efficient synthetic jet based on this consideration, which is the standard sinusoidal function with some modulation. This ideal is something like that of Lockerby and Carpenter [23], who proposed a pressure jump actuator driven by the step force. But the motivation of their studies is to minimize the risk of ingesting dust [23] and to control a quickly advecting streak in the turbulence boundary layer [24] which is totally different than ours. The objective of the present study is to investigate the effect of this novel signal pattern on the formation and evolution of the synthetic jet by numerical simulation; the unsteady characteristics and the mean flowfield of the synthetic jet actuated by this novel signal wave pattern are also presented.

II. Numerical Simulation Tool and its Validation

The governing equations used in the present study are the two-dimensional unsteady Reynolds-averaged Navier–Stokes equations, and they are solved by the commercial computational fluid dynamics software package Fluent. According to Tang and Zhong [25], the renormalized group (RNG) k–ε and the standard k–ω turbulence models could best match the experimental data, and so all the simulations in the present study are done by the standard k–ω turbulence model. Pressure implicit with splitting of operators (PISO) based on a higher degree of approximate relation between the iterative corrections for pressure and velocity is chosen. Although the PISO algorithm requires more CPU time, it greatly improves transient calculations as concluded by Tang and Zhong [25]. Second-order upwind spatial discretization is used for the momentum, turbulence kinetic energy, and turbulent dissipation rate. The orifice-wide D in the present study is 0.5 mm, and the height of the orifice is $D = 0.5$ mm. The cavity width and height are 40 and $16D$, respectively. Then the Helmholz frequency is

$$f = \frac{c}{2\pi}\sqrt{\frac{S}{VL}} = \frac{334}{2\pi}\sqrt{\frac{D}{40D \cdot 16D \cdot D}} = 4202.5 \text{ Hz}$$

which is much larger than the actuation frequency 200 Hz, and so we can use the incompressible flow equations to simulate the synthetic jet in the present study.

The no-slip (wall) boundary condition is applied for the bottom of the surrounding flowfield region, the orifice, and the cavity wall. The outflow condition is used at the top and sides of the surrounding flowfield ($\partial U/\partial y = 0, \partial V/\partial x = 0$). To model the perturbation of the flow from the oscillation motion of the actuator, a suction/blowing type boundary condition is used. The perturbation on the flowfield is introduced through the wall normal component of velocity at the oscillation membrane $U(t) = U_0 f(\eta)\sin(\omega t)$, where $f(\eta)$ is the different spatial variations over the orifice and η denotes the cross-stream direction. Kral et al. [26] suggested a "top hat" distribution closely matches the actual experiment, i.e., $f(\eta) = 1$. In the novel signal wave pattern, T_1 and T_2 represent the time duration of the blowing and suction cycles in one period, respectively, and the ratio of these two parameters is defined as the suction duty cycle factor $k = T_2/T_1$. According to this definition, $k > 1$ means the suction cycle is longer than the blowing cycle for the synthetic jet, and this signal wave pattern will generate a more efficient synthetic jet from the preceding analysis. To keep the constant parameters (L_0, Re_{U_0}) with different suction duty cycle factors, the velocity amplitudes at the oscillation membrane should be adjusted corresponding to the suction duty cycle factor. The use defined function in Fluent specified the velocity normal to the membrane is

$$U(t) = \begin{cases} \frac{k+1}{2}U\sin\left(\frac{k+1}{2}\omega(t-nT)\right) & nT \le t \le nT + \frac{T}{k+1} \\ \frac{k+1}{2k}U\sin\left(\frac{k+1}{2k}\omega(t-nT) + \frac{k-1}{k}\pi\right) & nT + \frac{T}{k+1} \le t \le (n+1)T \end{cases}$$

where $T = 1/f$ is the actuator oscillation cycle and U is the velocity amplitude with the suction duty cycle factor $k = 1$.

There are three cases simulated in the present study which have the suction duty cycle factor $k = 0.5$, 1, and 2. The actuator frequency of the synthetic jet is $f = 200$ Hz, and the stroke length ratio is $L_0/D = 26$. The characteristic blowing velocity is $U_0 = 5.2$ m/s, and this yields the Reynolds number based on the orifice width scale $Re_{U_0} = 356$. Because the periods of the blowing/suction cycle change with the suction duty cycle factor for the synthetic jet with equal actuator frequency, the time step is selected to insure the total time step numbers in the blowing or suction cycles are larger than 50 in each step. This results in that the time step numbers with $k = 0.5$ and 2.0 are 150, but that with $k = 1.0$ is 100. The convergence tolerance of continuity and two velocity components of 1E-5 and maximum iterations of 50 are set.

Tang and Zhong [25] have validated the capability of the standard k–ω turbulence model of Fluent in simulating the flowfield of synthetic jets in quiescent conditions. To make a further validation, we chose the experimental data of case 1 in the Langley Research Center workshop, "CFD Validation of Synthetic Jets and Turbulent Separation Control" [27] (CFDVAL2004) to verify the present simulation tool, which is a benchmark experiment in simulating the synthetic jet development in ambient conditions. The data used in the present study are the more recent experimental data using particle imaging velocimetry (PIV), hot wire, and laser Doppler velocimetry (LDV) by Yao et al. [28]. Because the LDV and PIV experimental data matched well, we just present the experimental data obtained by hot wire and LDV. The LDV data are scaled by a factor 0.9 suggested in the introduction file, because the amplitude of the membrane in

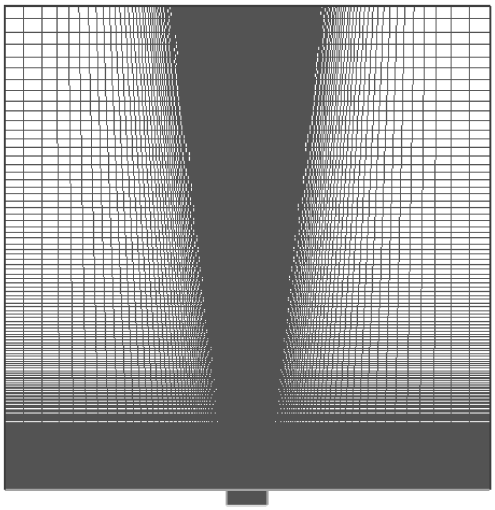

a) Whole grid

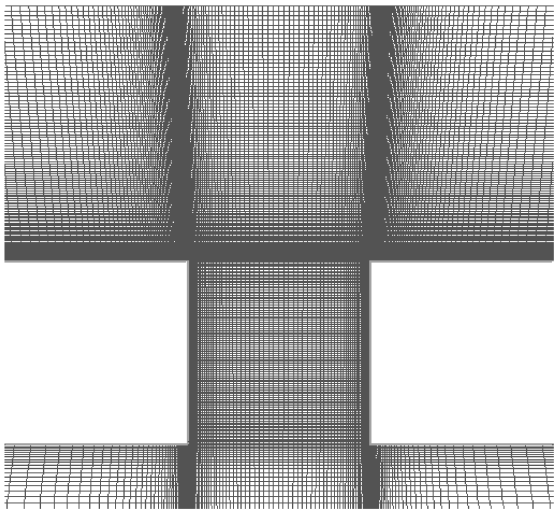

b) Near the orifice

Fig. 2 Medium grid system adopted in present simulation.

LDV measurement is larger than that in the hotwire experiment. To match the velocity fluctuation near the orifice well, we used the Fourier series to fit the velocity curve at $y = 0.3$ mm on the orifice centerline suggested by Vatsa and Turkel [29]. This treatment can reduce the discrepancy of the membrane boundary condition between the experiment and the simulation.

The simulation domain is the same as that suggested by CFDVAL2004 in case 1, and the differences are the geometry of the cavity and the membrane oscillation direction (as shown in Fig. 2). The effect of grid resolution on the solution has been examined. The structure of the two-dimensional grid one and two provided by the CFDVAL2004 are used as the coarse and medium grid systems in the present simulation, which have 46,000 and 17,800 grid points, respectively. The total grid points in the fine grid system are about 315,700. The grid distribution in these three grid systems are presented in Table 1. The streamwise velocity fluctuation in one cycle at three points, $y = 0.3$, 2, and 4 mm ($x = 0$), and the time-averaged streamwise velocity along the centerline calculated with three grid systems are plotted in Figs. 1 and 4, respectively. It is

Table 1 Three grid systems

Table 1	Cavity	Orifice	Surrounding
Coarse	100×60	49×60	192×193
Medium	150×100	73×100	433×361
Fine	200×133	100×133	571×483

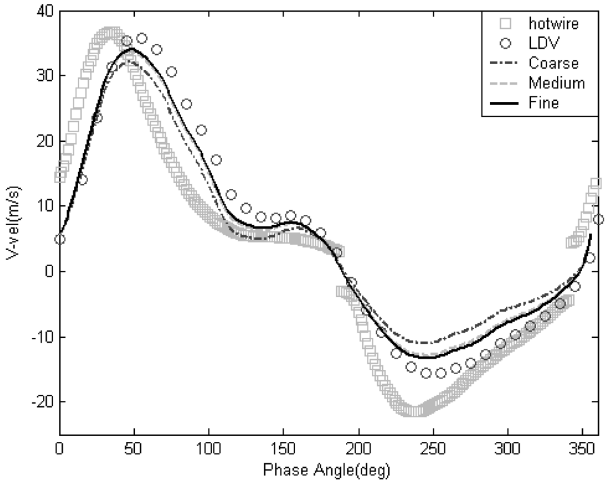

a) x=0, y=0.3mm

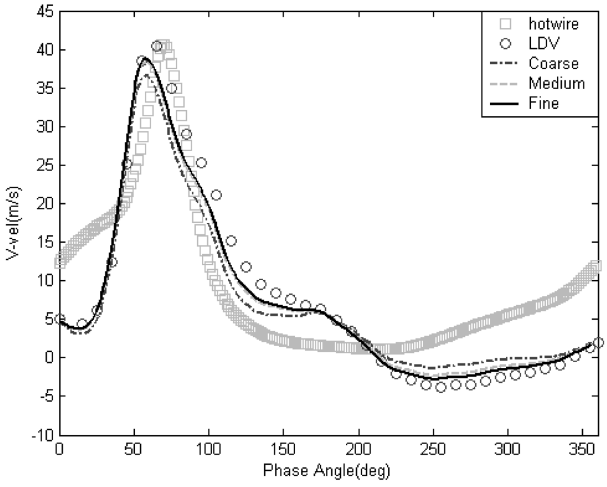

b) x=0, y=2mm

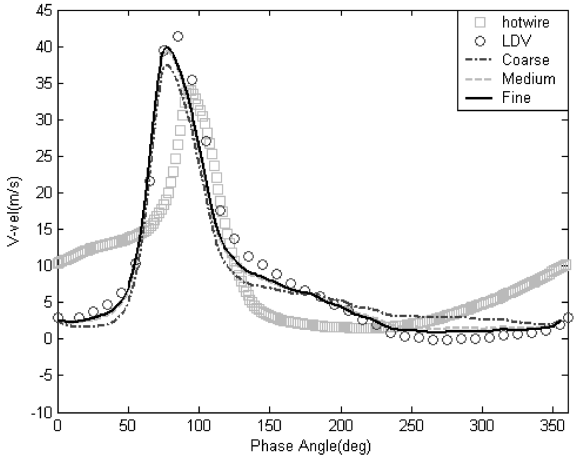

c) x=0, y=4mm

Fig. 1 Phase-averaged centerline velocity during one cycle for the validation case 1 of CFDVAL2004.

observed that the results calculated with the medium grid and find grid have almost no difference, but the velocity amplitude predicted with the coarse grid is a little less than the former two grid systems. Therefore, the medium grid is proper for the present study and is used in the following simulations. The scale of the computational domain and the density in the fine grid system are listed in Table 2, and the detail about the grid distribution can be seen in Fig. 2. Figures 1 and 4 also contain the experimental data measured by hotwire and LDV. The streamwise velocity fluctuation calculated in the present study

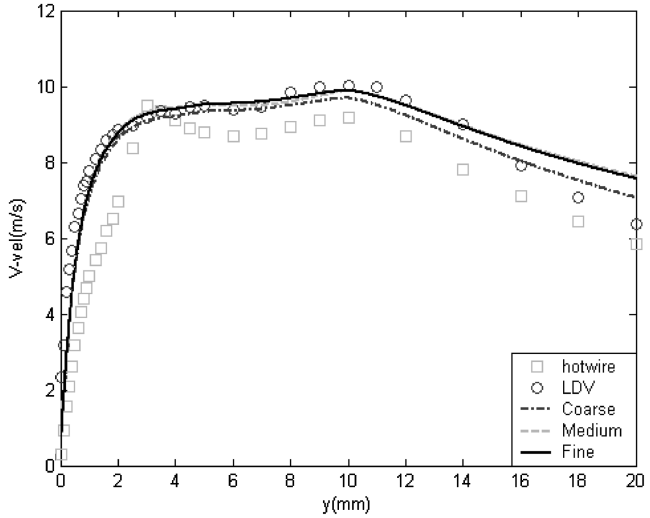

Fig. 4 Time-averaged centerline velocity for the validation case 1 of CFDVAL2004.

match well with the LDV data, but has some discrepancy with the hotwire data. This can be attributed to disturbance to the hot wire introduced by the velocity gradient and the heat transfer to the wall when the hot wire is applied in the boundary layer [26]. Figure 4 presents the comparison of the time-averaged streamwise velocity along the centerline. The simulation results are also coincident to the LDV data, except for a little overprediction in the region $y > 15$ mm. From the preceding discussion, it is concluded that the simulation tool and the grid system used in the present study are suitable to simulate the synthetic jet in static ambient air.

III. Formation and Evolution of Vortex in the Near Field

Figure 5 shows the vorticity contours during the blowing and suction cycles with the suction duty cycle factor $k = 0.5$, 1, and 2, and the vorticity levels used in the three cases are the same and the contour legends are omitted. The figures in left column are corresponding to the moment with the peak blowing velocity. It is obvious that the position and scale of the first vortex pair formed near the edge of the orifice have little difference in all these three cases. This result indicates that the position of the vortex pair is independent of the suction duty cycle factor k during the blowing cycle. It is well known that the stroke length ratio L_0/D is the key parameter determining the trajectory of the vortex pair and its convection velocity. The stroke length ratios L_0/D in our three cases, obtained by integrating the velocity during the blowing cycle, have the same value, and so the first vortex pair has the same trajectory during the blowing cycle. But the second vortex pair in the same figure appears at different positions; they are $Y/L_0 = 0.48$, 0.6, and 0.7 for $k = 0.5$, 1.0, and 2, respectively. The figures in the right column show the development of the first vortex pair, which presents the effect of the suction on the vortex pair formation.

The instant streamwise velocity $u_{\mathrm{cl}}(t)$ at 12 different stations in the region $Y/D = 0.1 \sim 16$ along the centerline are presented in Fig. 6. All the curves in the figure have a uniform vertical scale of $-5 \sim 5$, which is marked at the top of the figure. The variation of the streamwise velocity represents the movement of the vortex pair, and

Table 2 Scales of the computation domain and the grid density in the medium grid system

Zones	Geometry scale	Grid points	Min. horizontal grid size	Min. vertical grid size
Cavity	$40 \times 16D$	150×100	$0.0053D$	$0.0053D$
Orifice	$D \times D$	73×100	$0.0026D$	$0.0053D$
Surrounding	$480 \times 480D$	433×361	$0.0026D$	$0.0053D$

the moment when the peak velocity appears is corresponding to the vortex pair center just passing through the sample point. In the near field of the synthetic jet with $0.1 < Y/D < 4$, the peak blowing velocity increases in the streamwise direction, but the peak suction velocity decreases monotonically. Figure 7 shows the peak blowing velocity $u_{\mathrm{cl\,max}} = \max\langle u_{\mathrm{cl}}(t/T, Y/D)\rangle$ and the peak suction velocity $u_{\mathrm{cl\,min}} = \min\langle u_{\mathrm{cl}}(t/T, Y/D)\rangle$ vs the streamwise location Y/D. The maximum value of $u_{\mathrm{cl\,max}}$ which represents the location of the vortex pair fully formed appears at about $Y/D = 4$; meanwhile the peak suction velocity $u_{\mathrm{cl\,min}}$ induced by the suction of the orifice goes to zero. These indicate that the entrainment of the orifice to the ambient fluid during the suction cycle has vanished and the vortex pair has been fully formed. In the region with $4 < Y/D < 16$, there is more quiescent fluid entrained into the jet with the development of the vortex pair, which results in the decrease of $u_{\mathrm{cl\,max}}$ to satisfy the law of momentum conservation. Comparing the curves with different values of k in Fig. 6, it is obvious that the peak blowing velocity almost vanishes for $k = 0.5$ at $Y/D = 12$, but it also exists for $k = 2$ until $Y/D = 16$. Figure 7 presents that the peak blowing velocity $u_{\mathrm{cl\,max}}/U_0$ varies from 2.6, 3.7, to 5.9 with $k = 0.5$, 1.0, and 2.0. Based on the Biot–Savart law, it can be estimated that the strength of the corresponding vortex pair also increases with k. Thus, we can conclude that the position of the first vortex pair is not affected by the suction duty cycle factor, but the vortex pair strength is enhanced with the increase of k. Back to the discussion in preceding sections, the strength of the vortex pair depends on the Reynolds number Re_{U_0} based on the orifice scale and the characteristic blowing velocity U_0, and so the suction duty cycle factor k must have some relation with the Reynolds number Re_{U_0}. Now we recall the definition of the suction duty cycle factor k in Fig. 1b. Although the three cases have the same actuator frequency $f = 200$ Hz, the actual efficient frequency of the blowing cycle should be kf, which varies with the suction duty cycle factor k. Then it is easy to derive that the efficient Reynolds number for the vortex formation during the blowing cycle should be $Re^* = kRe_{U_0}$, which increases with k and results in the enhancement of the vortex pair.

Figure 8 shows the trajectories of the vortex pair in the present three cases and the results of Smith and Glezer [11]. The simulated trajectory for $k = 1.0$ in the present study matches well with the experimental data at $Re_{U_0} = 489$. The positions of the vortex pair at the end of the blowing cycle are marked with open circle symbols on the curves, and that in the right column of Fig. 4 are marked with open square symbols. It can be seen that the onset time of the first vortex pair varies with k, but the positions of the vortex pair in three cases have little difference during the blowing cycle, which is coincident to the conclusion from the vorticity contours in Fig. 4. During the suction cycle, the entrainment effect on the vortex pair decreases with k, so that the vortex pair can propagate further and then form an larger scale jet in the far field. The celerity velocity U_c of the vortex pair is determined by taking the time derivative of its trajectory. The variation of the celerity velocity (normalized by the characteristic blowing velocity U_0) with t/T for the vortex pairs is shown in Fig. 9. During the blowing cycle, the positions of vortex pair with different k have almost equal value, so the celerity velocity increases with k. This can be explained as the time length of the blowing cycle decreases with k. At the end of the blowing cycle ($t/T > 1/3$, 1/2, and 2/3 for $k = 0.5$, 1.0, and 2.0, respectively), the celerity velocities of the vortex pair begin to decrease sharply. For $k = 1.0$, the celerity velocity decreases like $(t/T)^{-2}$ (a straight line segment $m = -2$ is shown in Fig. 9 for reference), this result is coincident to that of Smith and Glezer [11]. For $k = 2.0$ and 0.5, the exponent factors m are -1.35 and -2.3, respectively. The decrease of celerity velocity becomes slow with k increase, which also indicates that the entrainment effect of the actuator on the vortex pair is diminished. From the effects of k during the blowing and suction cycles, we can know the following:

1) The suction duty cycle factor k does not affect the stroke length ration L_0/D, and so it has little influence on the trajectory of the vortex pair of the synthetic jet.

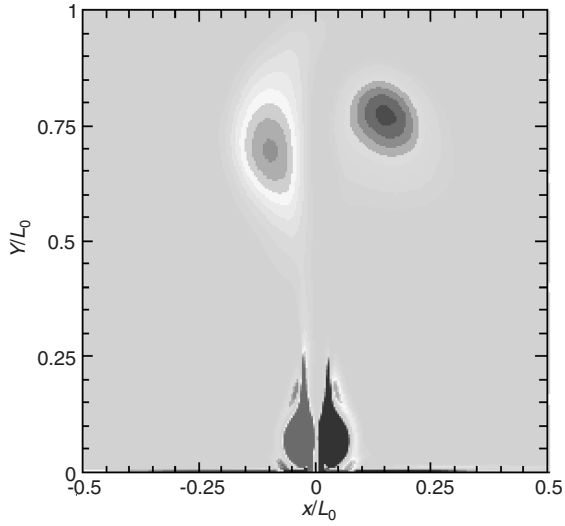

a) k=20, t/T=1/6

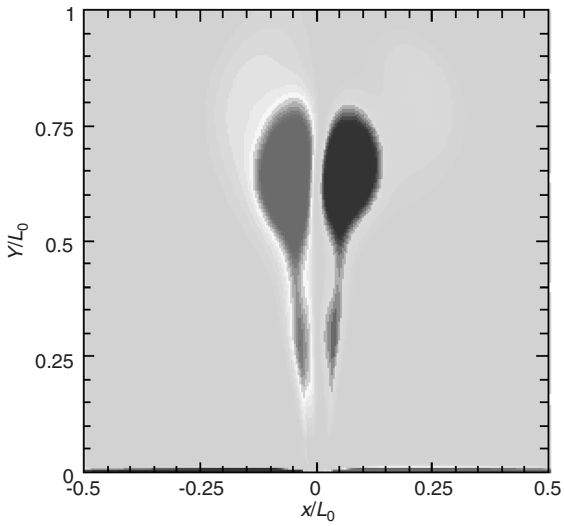

b) k=20, t/T=2/3

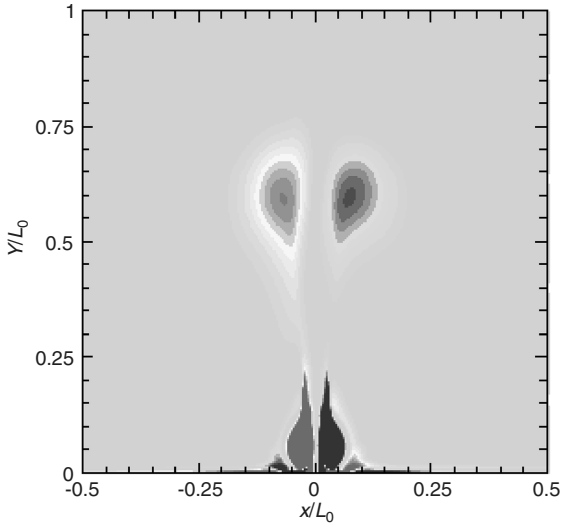

c) k=1.0, t/T=1/4

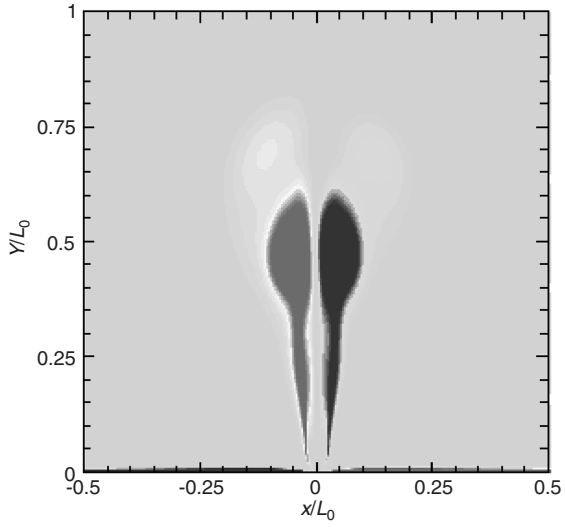

d) k=1.0, t/T=3/4

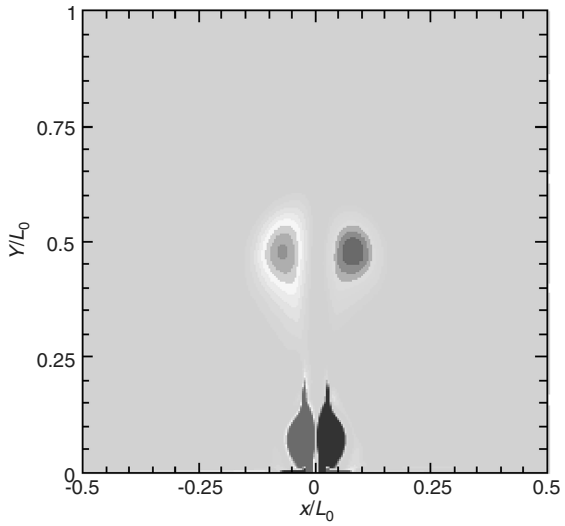

e) k=0.5, t/T=1/3

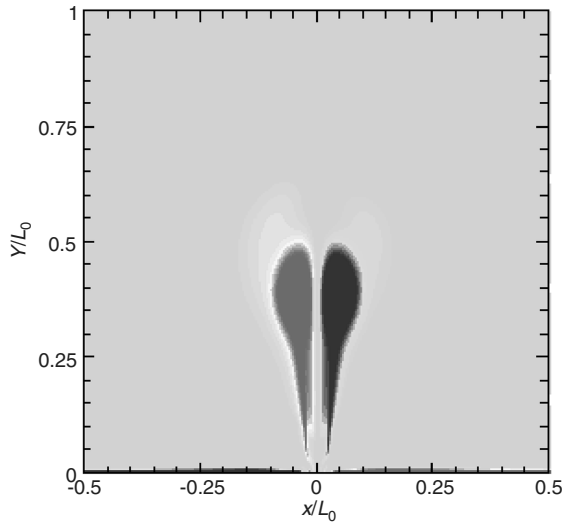

f) k=0.5, t/T=5/6

Fig. 5 Vortex structure during the blowing and suction cycles of the oscillation.

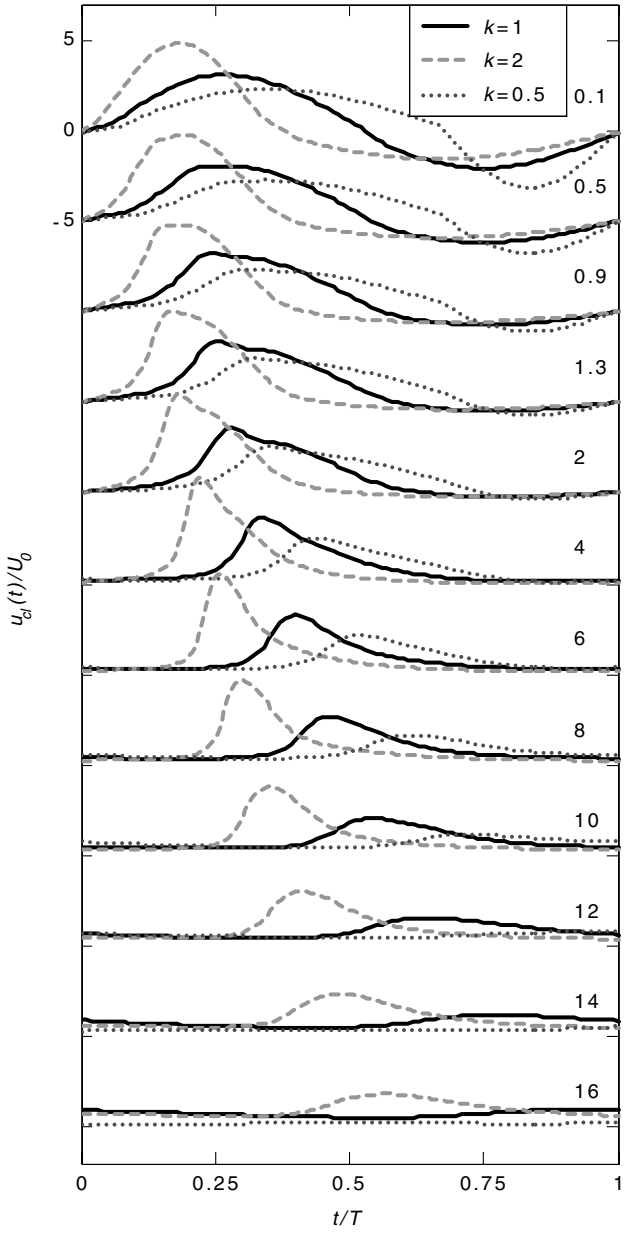

Fig. 6 Phase-averaged centerline velocity during one cycle with the indicated value of Y/D.

2) With the increase of k, the actual efficient Reynolds number Re^* increases, and the entrainment of the actuator on the vortex pair decreases. This leads to the vortex pair moving farther and forming a larger scale jet.

IV. Characteristics of the Mean Flowfield

Cross-stream distributions of the time-averaged streamwise velocity U with $k = 2.0$ are plotted in Fig. 10 (the velocity U is normalized by the time-averaged velocity along the centerline U_{cl}, and the cross-stream coordinate is normalized by the local jet width $b(x)$ based on $0.2U_{\mathrm{pp}}$; here U_{pp} is the peak-to-peak value of U). The dashed lines are the cross-stream distributions of U at 15 different streamwise stations with $Y/L_0 = 0.1 \sim 1$, and the dark line represents the hyperbolic cosine function $U = U_{\mathrm{cl}}\cosh^{-2}(\eta y)$ (where η is a parameter of the fit). Similar to the experimental results (Smith and Glezer [11], Smith and Swift [12]), the cross-stream distributions of the nondimensional streamwise velocity of the synthetic jet collapse reasonably well, and they match well with the hyperbolic cosine function. The cross distributions of time-averaged streamwise velocity with $k = 0.5$ and 1.0 have the same feature without being presented here.

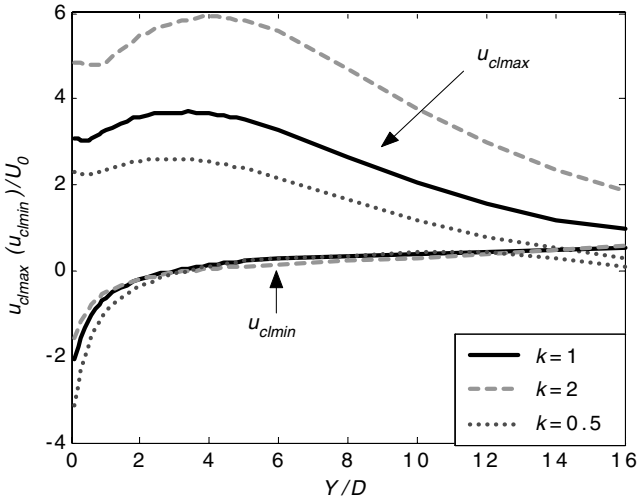

Fig. 7 Peak blowing velocity and peak suction velocity along the centerline of the synthetic jet.

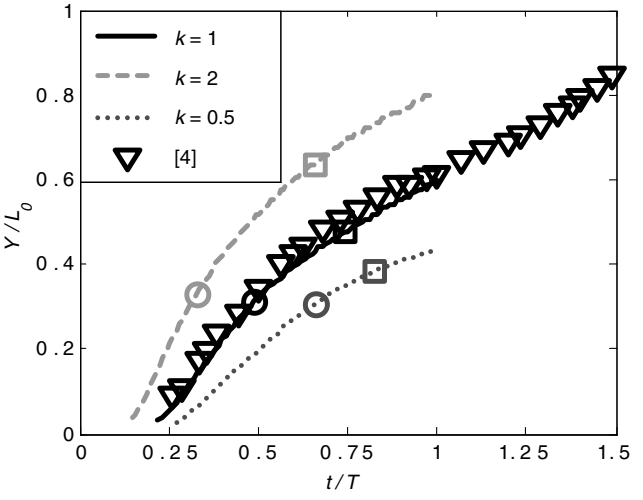

Fig. 8 Trajectories of the vortex pairs including data in Smith and Glezer [11].

The width b of the synthetic jet with $k = 0.5$, 1.0, and 2.0 at different streamwise stations are plotted in Fig. 11, in which the black line represents the power function curve with the factor $m = 1$. Except for the region near the orifice ($Y/D < 0.5$), the width of all jets grows linearly with the streamwise coordinate ($b \propto Y$). Smith and Glezer [11] indicated in their early study that the jet width b

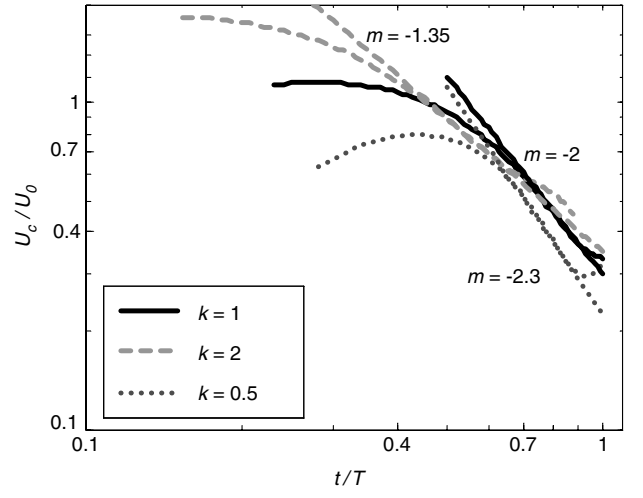

Fig. 9 Variation of vortex pair celerity velocity with nondimensional time.

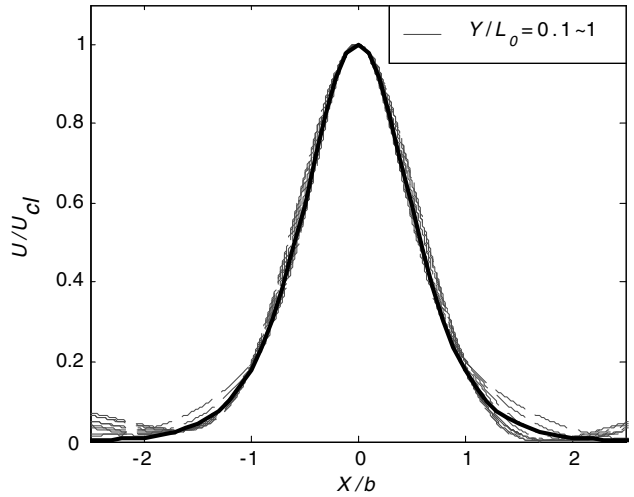

Fig. 10 Cross-stream distribution of streamwise velocity for $k = 2.0$ and fitted by the hyperbolic cosine function.

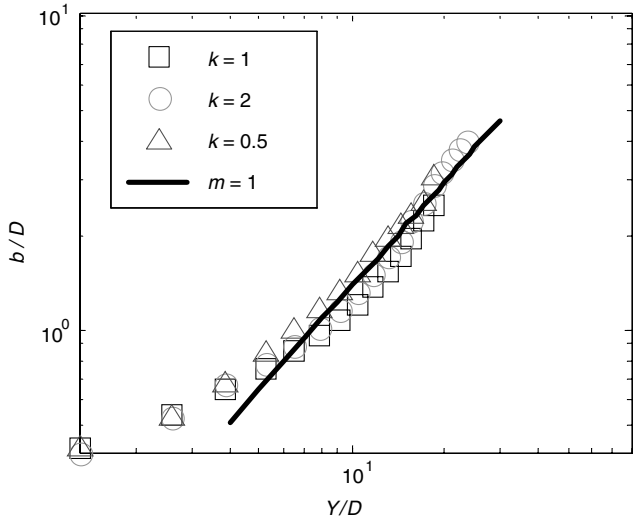

Fig. 11 Jet width (based on $0.2U_{pp}$) vs streamwise distance.

(based on $U_{cl}/2$) in the cross-stream plane increases like $Y^{0.88}$, but $b \propto Y$ for conventional two-dimensional jets. In recent studies on the comparison of synthetic jets and conventional continuous jets, Smith and Swift [12] argued that the cross-stream width b increases linearly with Y, which is reasonably coincident to the present study. From the characteristics of the synthetic jets with different k (the cross-stream velocity distributions of time-averaged streamwise velocity and the width of the jet), one can see that the flowfield actuated with different suction duty cycle factors is similar to that mentioned in previous studies.

Although the flowfields are similar for $k = 0.5$, 1.0, and 2.0, the scale and the strength of the vortex pairs have some difference, which has already been discussed. These differences also can be presented in the mean flowfield. Figure 12 shows the time-averaged streamwise velocity along the centerline U_{cl} with three different suction duty cycle factors. With $k = 0.5$ and 1.0, the time mean streamwise velocity grows faster at beginning, then it falls down slowly after the peak value before a more quick decrease. The time-averaged streamwise velocity with $k = 2.0$ keeps at a high level for $Y/D = 4 \sim 18$ after the increase onset. Another difference among these three jets is that they have different U_{cl} except in the region $Y/D < 4$, which is the vortex formation period of the synthetic jet. The synthetic jet with a larger value of k has a larger U_{cl} and can form a larger scale jet. The figure shows that the streamwise velocity with $k = 0.5$ decreases to zero at $Y/D = 20$, but it has a value of $0.1U_0$ with $k = 2.0$ at $Y/D = 30$.

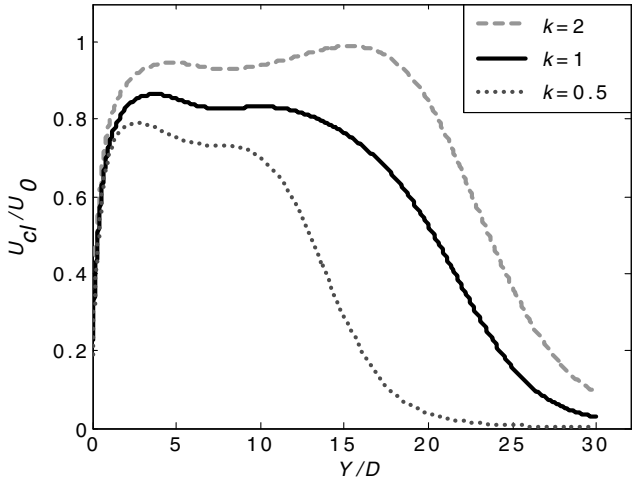

Fig. 12 Time-averaged centerline velocity vs streamwise distance.

V. Conclusions

The synthetic jet actuated by a novel signal wave pattern is studied numerically. The signal used in the present study is a modification mode from the standard sinusoidal function, which lengthens the time of the suction part and shortens the time of the blowing part in one oscillation cycle. A new parameter, the suction duty cycle factor k, is introduced to represent this modification. The formation and evolution of the vortex and the mean flowfield are presented. The following conclusions can be drawn:

1) The synthetic jets with different suction duty cycle factors have similar characteristics to that exhibited in previous studies; this means that the synthetic jet actuated by the novel signal wave pattern does not change its essential features.

2) The novel signal pattern proposed in the present study can generate a much stronger vortex pair, and so it can coalesce to synthesize a larger scale jet in the far field.

3) During the blowing cycle, the suction duty cycle factor just affects the strength of the vortex pair, but not the convection velocity and trajectory of the vortex. With a larger value of k, the strength of the vortex pair formed during the blowing cycle is increased.

4) The entrainment effect of the actuator cavity during the suction cycle on the vortex pair decreases with the increase of suction duty cycle factor k.

Acknowledgments

This project was granted financial support from the National Science Foundation of China under Grant No. 10602007 and the China Postdoctoral Science Foundation.

References

[1] Ingard, U., and Labate, S., "Acoustic Circulation Effects and the Nonlinear Impedance of Orifices," *Journal of the Acoustical Society of America*, Vol. 22, No. 2, 1950, pp. 211–218.

[2] Glezer, A., and Amitay, M., "Synthetic Jet," *Annual Review of Fluid Mechanics*, Vol. 34, 2002, pp. 503–529.

[3] Kiddy, J., Chen, P., Niemczuk, J., DeVoe, D., and Kiger, K., "Active Flow Control Using Microelectromechanical Systems," *AIAA/ASME/ASCE/AHS/ASC Structures, Structural Dynamics and Materials Conference and Exhibit, 41st, Atlanta, GA*, AIAA Paper 2000-1561, Apr. 2000.

[4] Amitay, M., Smith, D. R., Kibens, V., and Glezer, A., "Aerodynamic Flow Control over an Unconventional Airfoil Using Synthetic Jet Actuators, *AIAA Journal*, Vol. 39, No. 3, 2001, pp. 361–370.

[5] Amitay, M., and Glezer, A., "Role of Actuation Frequency in Controlled Flow Reattachment over a Stalled Airfoil," *AIAA Journal*, Vol. 40, No. 2, 2002, pp. 209–216.

[6] Amitay, M., and Glezer, A., "Controlled Transients of Flow Reattachment over Stalled Airfoils," *International Journal of Heat and Fluid Flow*, Vol. 23, No. 5, 2002, pp. 690–699.

[7] Hassan, A. A., and Janakiram, R. D., "Effects of Zero-Mass 'Synthetic' Jets on the NACA-0012 Airfoil," AIAA Paper 97-2326, 1997.
[8] Catalin, N., "Synthetic Jets Influence on NACA-0012 Airfoil at High Angles of Attack," AIAA Paper 98-4523, 1998.
[9] Holman, R., Gallas, Q., Carroll, B., and Cattafesta, L., "Interaction of Adjacent Synthetic Jets in an Airfoil Separation Control," AIAA Paper 2003-3709, 2003.
[10] James, R. D., Jacobs, J. W., and Glezer, A., "Round Turbulent Jet Produced by an Oscillating Diaphragm," *Physics of Fluids*, Vol. 8, No. 9, 1996, pp. 2484–2495.
[11] Smith, B. L., and Glezer, A., "Formation and Evolution of Synthetic Jets," *Physics of Fluids*, Vol. 10, No. 9, 1998, pp. 2281–2297.
[12] Smith, B. L., and Swift, G. W., "Comparison Between Synthetic Jets and Continuous Jets," *Experiments in Fluids*, Vol. 34, No. 4, 2003, pp. 467–472.
[13] Fugal, S. R., Smith, B. L., and Spall, R. E., "Displacement Amplitude Scaling of a 2-D Synthetic Jet," *Physics of Fluids*, Vol. 17, No. 4, 2005, pp. 045103.1–045103.10.
[14] Shuster, J. M., and Smith, D. R., "Study of the Formation and Scaling of a Synthetic Jet," *42nd AIAA Aerospace Sciences Meeting and Exhibit, Reno, Nevada*, AIAA Paper 2004-90, Jan. 2004.
[15] Holman, R., Utturkar, Y., Mittal, R., Smith, B. L., and Cattafesta, L., "Formation Criterion for Synthetic Jets," *AIAA Journal*, Vol. 43, No. 10, 2005, pp. 2110–2116.
[16] Smith, B. L., Trautman, M. A., and Glezer, A., "Controlled Interactions of Adjacent Synthetic Jets," AIAA Paper 99-0669, 1999.
[17] Guy, Y., McLaughlin, T. E., and Albertson, J. A., "Effect of Geometric Parameters on the Velocity Output of a Synthetic Jet Actuator," AIAA Paper 2002-0126, 2002.
[18] Milanovic, I. M., and Zaman, K. B. M. Q., "Highly Inclined Jets in Cross-Flow," AIAA Paper 2003-0183, 2003.
[19] Zhong, S., Garcillan, L., and Wood, N. J., "Dye Visualization of Inclined and Skewed Synthetic Jets in a Cross-Flow," *Aeronautical Journal*, Vol. 109, No. 2, 2005, pp. 147–155.
[20] Ritchie, B. D., Mujumdar, D. R., and Seitzman, J. M., "Mixing in Coaxial Jets Using Synthetic Jet Actuators," AIAA Paper 2000-0404, 2000.
[21] Mossi, K., Castro, N. D., Bryant, R., and Mane, P., "Boundary Condition Effects on Piezo Synthetic Jets," *Integrated Ferroelectrics*, Vol. 71, No. 1, 2005, pp. 257–266.
[22] Vukasinovic, B., Lucas, D. G., and Glezer, A., "Direct Manipulation of Small-Scale Motions in a Plane Shear Layer," AIAA Paper 2004-2617, 2004.
[23] Lockerby, D. A., and Carpenter, P. W., "Modeling and Design of Microjet Actuators," *AIAA Journal*, Vol. 42, No. 2, 2004, pp. 220–227.
[24] Lockerby, D. A., Carpenter, P. W., and Davies, C., "Control of Sublayer Streaks Using Microjet Actuators," *AIAA Journal*, Vol. 43, No. 9, 2005, pp. 1878–1886.
[25] Tang, H., and Zhong, S., "Two-Dimensional Numerical Study of Circular Synthetic Jets in Quiescent Flows," *Aeronautical Journal*, Vol. 109, No. 2, 2005, pp. 89–97.
[26] Kral, L. D., Donovan, J. F., Cain, A. B., Cary, A. W., "Numerical Simulation of Synthetic Jet Actuators, AIAA Paper 97-1824, 1997.
[27] Anon., "CFD Validation of Synthetic Jets and Turbulent Separation Control," Langley Research Center Workshop, http://cfdval2004.larc.nasa.gov [retrieved 20 April 2006].
[28] Yao, C. S., Chen, F. J., Neuhart, D., and Harris, J., "Synthetic Jet Flowfield Database for CFD Validation," AIAA Paper 2004-2218, 2004.
[29] Vatsa, V. N., and Turkel, E., "Simulation of Synthetic Jets Using Unsteady Reynolds-Averaged Navier—Stokes Equations," *AIAA Journal*, Vol. 44, No. 2, 2006, pp. 217–224.

G. Candler
Associate Editor